Journal of Nuclear Materials 394 (2009) 102–108

Contents lists available at ScienceDirect

Journal of Nuclear Materials

journal homepage: www.elsevier.com/locate/jnucmat

Creep-to-rupture tests of T91 steel in flowing Pb–Bi eutectic melt at 550 °C

A. Jianu [a,*], G. Müller [a], A. Weisenburger [a], A. Heinzel [a], C. Fazio [b], V.G. Markov [c], A.D. Kashtanov [c]

[a] Forschungszentrum Karlsruhe GmbH, Institute for Pulsed Power and Microwave Technology, P.O. Box 3640, D-76021 Karlsruhe, Germany
[b] Forschungszentrum Karlsruhe GmbH, Program Nuclear Safety Research, P.O. Box 3640, D-76021 Karlsruhe, Germany
[c] Central Research Institute of Structural Materials – "Prometey", 49 Shpalernaja, St. Petersburg, 191015, Russia

ARTICLE INFO

Article history:
Received 18 December 2008
Accepted 17 August 2009

ABSTRACT

Uniaxial creep-to-rupture tests were performed on T91 in air and in flowing lead–bismuth eutectic melts. Compared to specimens tested in air, the specimens tested in liquid–metal show: (i) strain and strain rate increase up to a factor of about 50 (strain rate); (ii) time-to-rupture decrease; (iii) rapid transition into the third creep stage at high stress (above 180 MPa). The analysis of the test results revealed several important surface phenomena, which lead to different behavior of the specimens tested in lead–bismuth eutectic melts compared to those tested in air. Under high stress, and therefore high strain, the crack propagation process is mostly controlled by the reduction of the surface energy due to Pb and Bi adsorption on the steel surface. Under low stress (140 and 160 MPa) and low strain, this process is delayed due to the competing mechanism of healing the oxide scale cracks.

1. Introduction

Lead–bismuth eutectic melts (LBE) are considered as working fluids for advanced nuclear applications such as accelerator driven systems (ADS) [1] and Lead Fast Reactors (LFRs) of GEN IV [2] due to their thermal and neutronic properties. The advantages of LBE as a coolant in fast neutron nuclear systems are discussed in Ref. [3].

Concerns related to the use of LBE arise from the materials compatibility, in terms of corrosion and mechanical resistance. The reference structural materials selected for the Heavy Liquid–Metal (HLM) cooled systems are 9Cr ferritic–martensitic (F/M) steels for core components and the austenitic steel AISI 316L for vessel and in-vessel structures. Previous studies showed that the corrosion mechanism of these steels in LBE is affected by several parameters, as e.g. the oxygen activity in the liquid–metal and the temperature. With appropriate oxygen activity in the liquid–metal, dissolution of steel elements in the liquid–metal can be minimized or suppressed through the formation of a protective oxide scale on the steel surface [4–10]. As far as the temperature effect is concerned, it was shown that austenitic steels suffer from severe corrosion attack in lead or LBE melt at temperatures above 500 °C, while F/M steels form thick oxide scales, that may spall off periodically and, eventually, block the cooling channels. Furthermore, the thick oxide scale hinders the heat transfer through the cladding wall of the fuel pins. Both materials are therefore restricted to application at temperatures below 500 °C [8].

The mechanical properties degradation of the structural materials can be described through Liquid–Metal Embrittlement (LME) and/or Stress Corrosion Cracking (SCC) mechanisms [11,12]. LME is the catastrophic degradation of mechanical properties of a normally ductile metal, when in contact with a liquid–metal under mechanical loading [13–15]. LME and SCC are similar with respect to stress, which must be present. However, the propagation of the fracture is much faster in LME than in SCC. In experimental studies of LME it is usually concluded that the observed crack propagation rates are too high to be accounted for by the diffusion process only. LME is considered as one of the well established manifestations of the Rebinder effect [16]. Accordingly, LME is based on a reduction of the surface energy by the adsorption of the atoms of the embrittling liquid–metal, which reduces the stress required for crack propagation, in accordance with Griffith theory [17,18].

There is evidence that the phenomena associated with failure can include: (i) cracking induced by the adsorption of liquid–metal atoms, (ii) accelerated failure due to the penetration of the liquid–metal along the grain boundary of the solid and (iii) stress-aided dissolution of metal from a crack tip. The particular role of the liquid phase, therefore, may be as an adsorbent, a penetrant or a solvent operating at a crack tip [19].

There is little doubt that the liquid–metal in a crack tip is adsorbed along strained atomic bonds, thereby lowering the binding energy of the atomic bonds [20]. However, work is still needed to clarify the very old and tricky problem of the embrittlement of ductile metals by liquid–metals [21].

* Corresponding author. Tel.: +49 7247 82 8519; fax: +49 7247 82 2256.
E-mail address: adrian.jianu@ihm.fzk.de (A. Jianu).

0022-3115/$ - see front matter © 2009 Elsevier B.V. All rights reserved.
doi:10.1016/j.jnucmat.2009.08.013

The aim of this work is to investigate the influence of the LBE environment on the creep-to-rupture properties of the 9Cr F/M "T91" steel. The "T91" steel has been selected as one of the candidate materials for neutron spallation target (ADS) and core components (ADS and LFR) because of its good mechanical strength and irradiation resistance in a fast neutron or a spallation spectrum. Of special relevance is the behavior of this material under long term loading and exposure to LBE in the 400–550 °C temperature range [3]. In this work creep-to-rupture tests are conducted under equal stress conditions in air and flowing LBE.

2. Experimental

The T91 material used in the creep-to-rupture experiments is a modified 9Cr steel with additions of Nb and V, to increase the mechanical strength, especially at higher temperatures. The measured yield strength at 450 °C in air is 440 MPa [22]. Before the test, T91 has been normalized at 1050 °C for 30 min and air quenched, followed by tempering at 770 °C for 1 h. Specimens were machined (gauge length of 70 mm and diameter of 6 mm) and grinded with 800 grit abrasive paper (Fig. 1).

The creep-to-rupture tests in uniaxial mode were performed at CRISM "Prometey". Specimens were tested at 550 °C, in air and in LBE, at uniaxial tensile stress levels of 140, 160, 180, 200 and 220 MPa. The LBE contained 10^{-6} wt.% oxygen at a flow rate of 0.5 m/s. A calibration curve was constructed from measurements in air, considering the elongation measured outside the test section (including contributions from the clamps and the bellows) and the direct elongation of the specimens. This calibration curve is applied to the tests in LBE, where only the elongation outside the test section can be measured. Before applying the stress, the specimens were kept in LBE, for 100 h at the test temperature, to pre-oxidize surfaces and to release stresses. Data points were logged every 6 h for long duration experiments. Two specimens were simultaneously tested in LBE, at two different stress levels, and extracted together from the LBE. Due to different rupture times, only one specimen was extracted immediately after the rupture, while the rupture surface of the other specimen was exposed to LBE for some additional time.

After completion of the tests, specimens were cut from the samples, one centimeter away from the fracture surface and parallel to it. Hot oil and a mixture of CH_3COOH, H_2O_2 and C_2H_5OH at a ratio of 1:1:1 were used to remove the LBE adherent from the specimen's surfaces. The fracture surface, the lateral surface and the cross section of the specimens were examined with the Hitachi S800 scanning electron microscope in the secondary electron mode (SEM-SE). The EDX analysis was performed with the Thomson WIN EDS attached to the Hitachi S800.

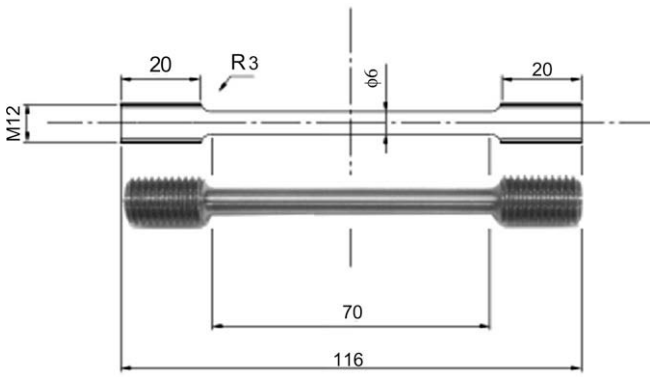

Fig. 1. Scheme and photograph of the specimens.

3. Results

3.1. Creep-to-rupture tests

For a better comparison, strain versus time plots of the creep tests, performed in air and in LBE, are shown in Fig. 2A and B for high and low stress, respectively. For all stress levels, the creep tests performed in LBE at 550 °C show that strain and strain rate increase and the time-to-rupture decreases for the samples exposed to LBE, in comparison with the results obtained with specimens tested in air (Figs. 2 and 3). Rupture was observed only after 10,000 h of exposure for specimens tested in air at stresses of 180 MPa and below. The time-to-rupture of the 200 MPa and 220 MPa specimens (the latter not depicted in the diagram) tested in air are similar to those described in the literature [23]. The test at 140 MPa in LBE was terminated after 4500 h without rupture at

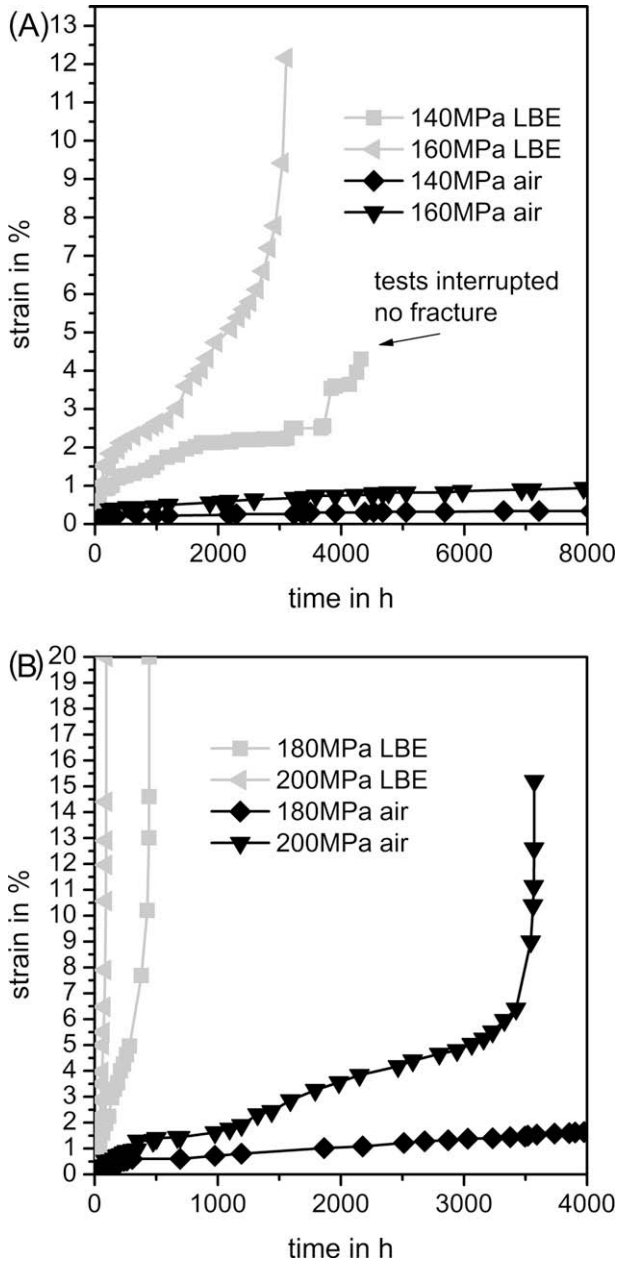

Fig. 2. Comparison of creep to rupture diagrams of T91 in LBE and in air at 550 °C, (a) 140 and 160 MPa, (b) 180 and 200 MPa.

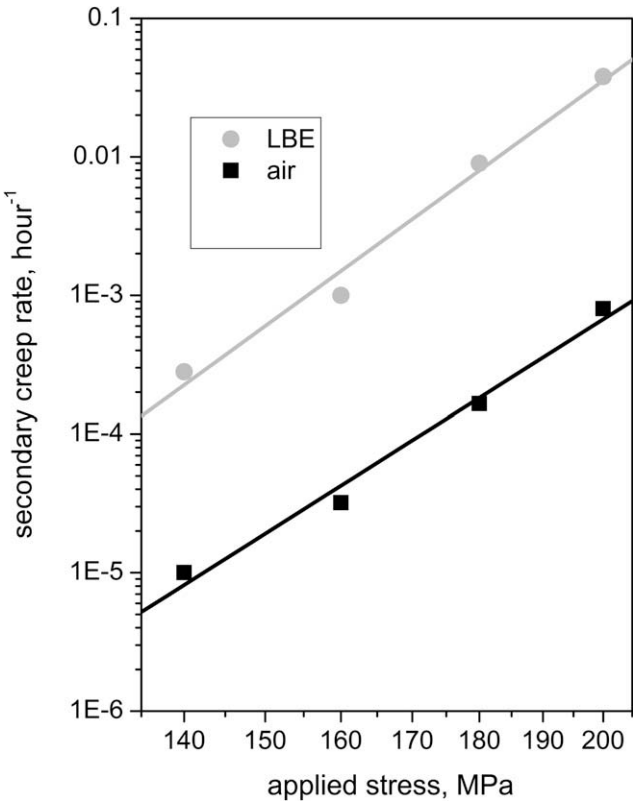

Fig. 3. Comparison of secondary creep rate of T91 tested at 550 °C in air and LBE.

a strain of about 4%. All the other experiments in LBE were continued until rupture occurred.

The measured time-to-rupture, for the specimens exposed in LBE, is significantly shorter than that for the ones in air (Fig. 2). Compared to the specimens tested in air, for all the specimens tested in LBE, the strain (%) in the primary creep phase is higher and the onset of secondary creep occurs earlier. The specimens tested in LBE show an earlier transition into the third stage of creep and a decrease of the duration of the steady-creep stage (2nd creep). Although the duration of the 2nd creep stage is shorter, the strain is significantly higher. For all the applied stresses, the secondary creep rate is significantly lower for the specimens tested in air than for those tested in LBE, as depicted in Fig. 3.

The fitted curves for LBE and air were finally taken to calculate the ratio of the 2nd creep rates of specimens tested in LBE and in air (Table 1). The influence of LBE on the creep strength is clearly stress-dependent. At 200 MPa, the creep is about 53 times faster in LBE than in air, at 140 MPa this ratio drops to 27.

3.2. Metallographic analysis

Metallographic examinations have been performed only on the broken specimens.

Table 1
Ratio of 2nd creep rates for T91 at 550 °C tested in air and LBE.

Stress [MPa]	Ratio of 2nd creep rates, LBE/air
140	27
160	35
180	44
200	53

3.2.1. Samples tested in air

Fractographic analysis was performed in order to determine the main macroscopic and microscopic features of the broken specimens.

The specimens tested in air show necking regions and cup-and-cone fracture surfaces (Fig. 4A). The fracture surfaces consist of many microvoids and of dimples, a morphology specific to ductile-type fracture surfaces (Fig. 4B).

The lateral surface of the specimens is covered by a rough and irregular oxide scale. In the necking region, a preferential orientation of the oxide scale along the longitudinal axes of the specimens was observed at macroscopic level. As shown in Fig. 5 (sample exposed to 200 MPa as a representative for all specimens tested in air), the scale has an inhomogeneous aspect: an outer region with cracks and tendency to spall and an inner region, continuous and adherent to the steel surface. It was assumed that the brittle oxide layers crack under the applied loads, but the cracks stop at the steel–oxide interface and do not affect the steel substrate. The steel surface at the crack tip develops again a thin oxide scale.

3.2.2. Samples tested in LBE

The samples exposed to LBE, under 160 and 180 MPa loads, show a fracture surface inclined with 40–50° versus the longitudinal axis (Fig. 6A). The specimen fracture surface exposed to 200 MPa in LBE (Fig. 6B) is perpendicular to the direction of the applied load, while the specimen exposed to 220 MPa (LBE) shows a cup-and-cone shape fracture surface (Fig. 6c). All specimens show necking regions.

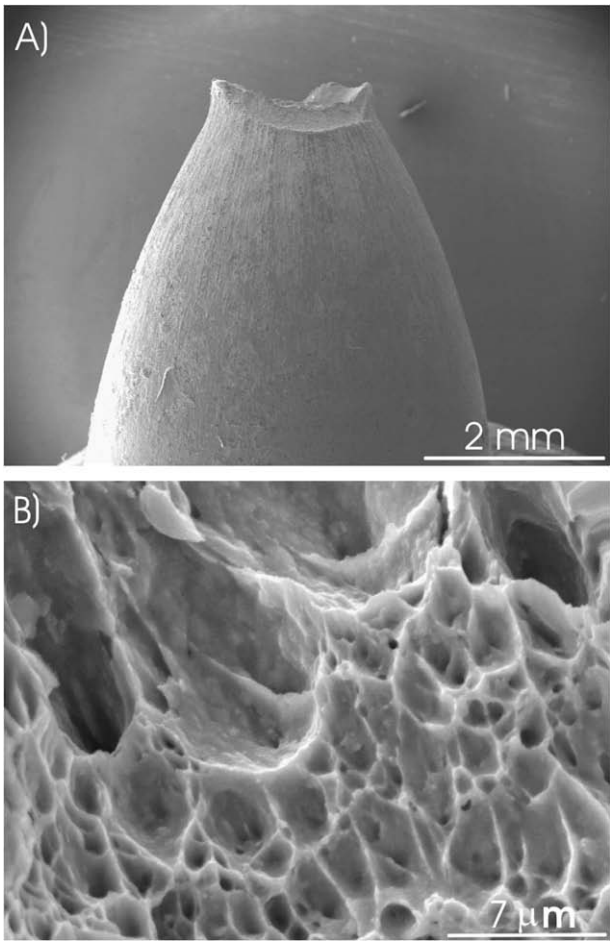

Fig. 4. Necking region (A) and details of ductile fracture surface (B) of a sample tested in air at 200 MPa.

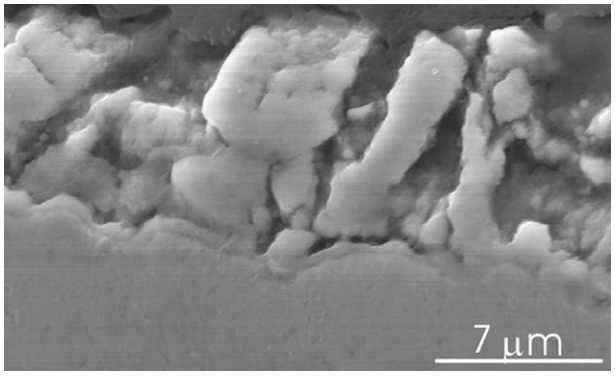

Fig. 5. Details of the typical scale formed on the specimens tested in air, with cracks in the outer regions and self healed scale on the steel surface.

Due to the conditions set by the creep test facility, the specimens were not extracted from LBE immediately after they were broken (with one exception). Therefore the fresh fracture surfaces were exposed to LBE melt and the microscopic features, which characterize the type of the fracture behavior, were altered. However, the sample exposed to 220 MPa load was immediately extracted from the test facility and the microscopic features could be observed. Two different aspects of the fracture surface of this specimen were observed: (i) an internal region with microvoids and dimples surrounded by a shear fracture surface (ductile-type fracture feature) and (ii) a small peripheral region exhibiting a flat morphology, which could be related to brittle-type fracture.

In the necking region of the sample exposed to 160 and 180 MPa in LBE, areas with oxide scale scraps, surrounded by regions with dissolution attack, were observed (Fig. 6A). Under the experimental conditions, parts of the oxide scale may have been removed from the specimen surface. For the sample exposed to 200 MPa in LBE, this phenomenon is limited to the region close to the fracture surface (Fig. 6B), while it is totally absent for the sample exposed to 220 MPa in LBE (Fig. 6C).

Multiple microcracks in the oxide scale were observed on the lateral surfaces of the specimens. The density, width, depth and orientation of these microcracks depend on the applied load and on the distance from the fracture surfaces. The number, width and the depth of these microcracks decrease with increasing distance from the fracture surfaces, because the deformation of the samples decreases also in these regions (Fig. 7).

Close to the fracture surface, the sample exposed to 160 MPa shows deep microcracks (Fig. 8A), surrounding the sample and oriented perpendicular to the stress direction. At higher stresses their density increases, the orientation is random and they are less deep (Fig. 8B). It can be assumed that such a microcrack plays an essential role in the behavior of the samples: the onset of necking period and of the final fracture (Fig. 8C).

The samples exposed to 160 and 180 MPa show dissolution attack at the bottom of the deepest microcracks, close to the top of the necking region, where the deformation of the sample is larger (liquid–metal penetrates into the steel along these microcracks). Dissolution attack occurs also on the lateral surface of the neck, close to the fracture surfaces, where scale delaminates (160 and 180 MPa). An EDX point analysis, performed in such regions, indicates the depletion in chromium content to values in the 3–5 wt.% range. Oxygen has not been detected and the repassivation did not happen, showing that the steel surface was exposed directly to LBE melt depleted in oxygen.

The small and less deep cracks in the samples exposed to 180–220 MPa show a different aspect (Fig. 9A and B). Pores at grain boundary junctions and intergranular cracks (Fig. 9A), transgranular cracks (Fig. 9B), intergranular penetration of LBE, depletion of Cr and partial healing of the oxide scale were observed.

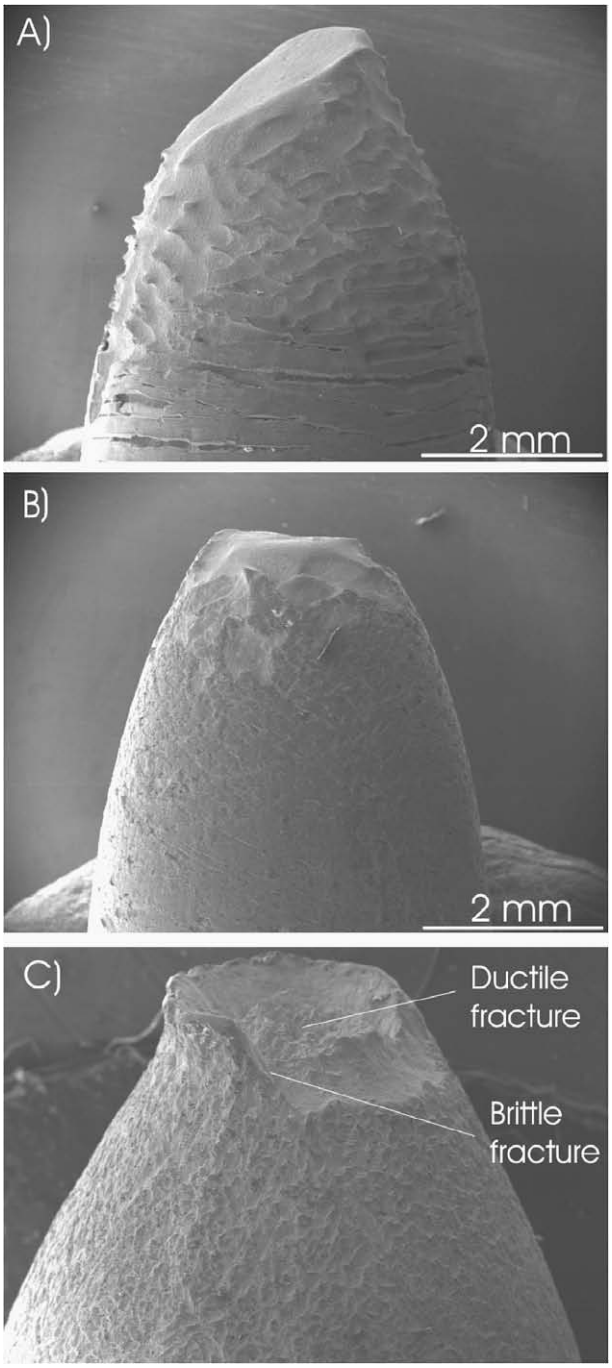

Fig. 6. Examples of the necking regions and fracture surface of the specimens tested in LBE: fracture surface, inclined with 40–50°, of the specimen tested at 160 MPa (A); almost horizontal fracture surface of the specimen tested at 200 MPa (B); cup-and-cone shape fracture surface of the specimen tested at 220 MPa (C).

SEM examination of the cross sections was also carried out in order to estimate the scale morphology, to identify the elements incorporated in the oxide scale and to evaluate the crack propagation and LBE penetration at the microcrack tips.

All samples exhibit an oxide scale with multilayer morphology. EDX analyses indicate three layers: an outer magnetite layer, an inner Fe–Cr spinel-type oxide layer and an innermost internal oxidation zone (IOZ) with Cr-depleted grains (4–6 wt.%). The magnetite layer tends to spall off and the entire scale lost adherence and was

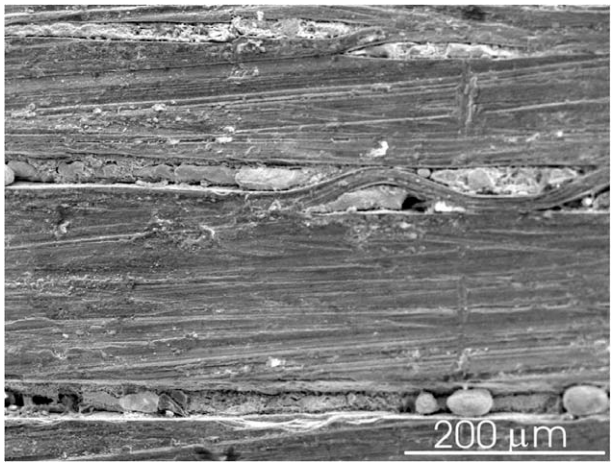

Fig. 7. Example of cracks observed on the surface of the sample exposed at 160 MPa far from fracture surface (approx. 1 cm).

removed in many parts of the necking regions (especially close to the fracture surface).

At the interface between IOZ and the spinel-type layer, a region with pores is present. The numbers of these cavities, as well as the thickness of these regions, increase with the applied loads. A chromium-rich (30–40 wt.% Cr) spinel-type oxide is bordering the pores.

The multilayered oxide scales show many microcracks (Fig. 10). The cracks, observed in the oxide scales, are initiated in the external sublayer and either stop at the interface between the two sublayers or cross also into the internal sublayer. The microcracks, located far from the fracture surface (low strain), are blocked by a probably renewed scale (section I in Fig. 10). But the tips of the microcracks, located close to the fracture surface (in the highly deformed region of the neck), show LBE penetration into regions with porosities and along grains boundaries, leading to dissolution attack (section II in Fig. 10).

4. Discussion

The creep-to-rupture time for the specimens exposed to air is very similar to literature values [23]. This indicates that typical creep mechanisms of F/M steels, like dislocation-glide, vacancy and void-formation, viscous creep and grain boundary sliding, take place.

However, the behavior of specimens under high uniaxial stresses is very different when exposed to LBE environment (Fig. 11). The time-to-rupture of specimens tested in LBE is significantly smaller compared to the one of specimens tested in air. As shown in the diagrams in Fig. 2, the stress–strain curve of the specimens in LBE starts with a steep slope already at the beginning of the test, while for the specimens exposed to air, it starts with a flat course. Additional to the known creep mechanism, a strong surface effect is visible. Since the specimens in LBE are covered by a protective oxide scale formed before stress was applied, one has to assume that the scale brakes in a very early stage, thus allowing access of the LBE to the bulk material. Obviously, the LBE that reaches the scale crack tip becomes depleted in oxygen, which prevents formation of an oxide scale on the crack tip, with the result of lowering the surface energy (Rebinder effect), dissolution attack and propagation of the crack.

Macroscopic and microscopic investigations of the LBE-exposed specimens revealed that three factors lead to a direct contact between LBE and the unprotected steel surface, dissolution attack and crack propagation. These factors are: (i) thick and brittle oxide scales, (ii) pores between oxide scale and IOZ and (iii) Cr-depleted grains in the IOZ.

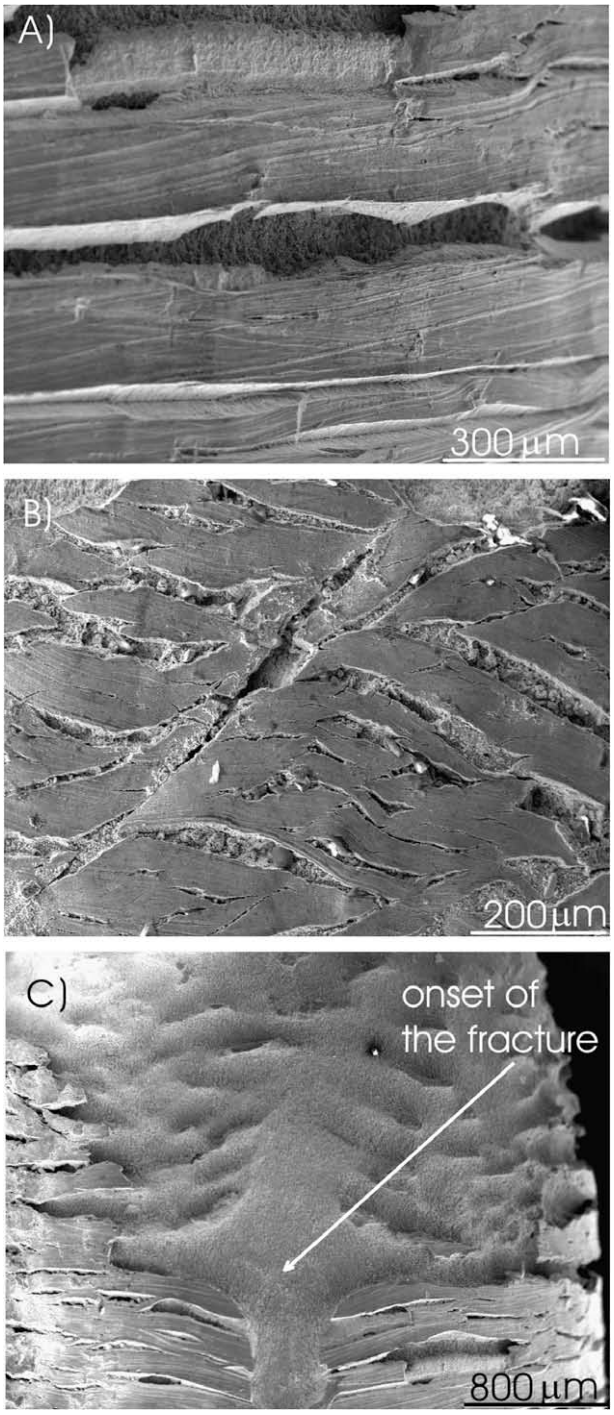

Fig. 8. Microcracks on the lateral surface of the specimens: deep microcracks in the necking region, surrounding the sample tested with 160 MPa (A); random oriented microcracks on the surface of specimen tested with 180 MPa (B) and crack considered as starting point of the final failure of the sample tested with 160 MPa (C).

Under the applied loads, the oxide scale, that is harder and thus less ductile than the steel, breaks. At low stress values (equivalent to low strain), the number and the size of the cracks are relatively small. If the crack opening is too small or the crack does not reach the steel interface, the LBE does not come in direct contact with the steel and a new oxide scale gradually covers the surface of the tip, blunting the crack and blocking the direct contact of LBE with steel

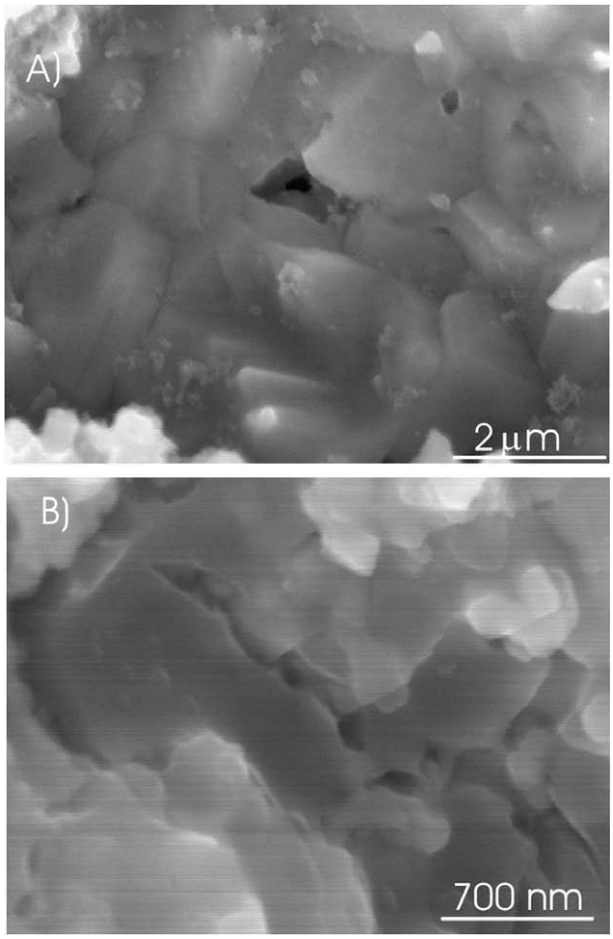

Fig. 9. Morphological aspects of the bottom regions of the microcracks observed on the lateral surface of the necking region: voids, intergranular cracks – 180 MPa (A); transgranular microcrack – 200 MPa (B).

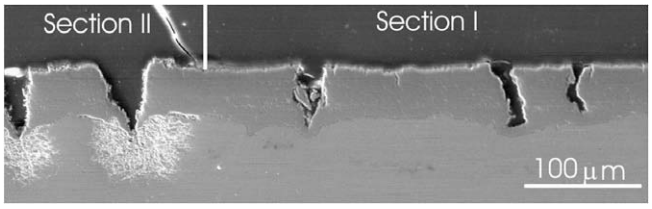

Fig. 10. Microcracks observed in the sample exposed to 160 MPa far from fracture surface (section I) and at the beginning of the necking region (section II).

(Fig. 10, section I). In cases with lower applied stresses (140 and 160 MPa), the first and the second creep stages are relatively long compared to higher stress. The influence of the LBE, that is expressed in the ratio of the 2nd creep rate in LBE and in air (see Table 1), drops from 53 at 200 MPa to 27 at 140 MPa. It appears that, under a certain low value of stress applied to steel samples exposed to LBE, there will be no scale damage to give direct access of LBE to the steel. Therefore, it may be justified to extrapolate the data obtained during creep tests in air in order to define the creep-to-rupture behavior of steel specimens exposed to LBE, below a certain stress level, where no scale cracking occurs. Such behavior was observed in [24] for Cr-steel containing 1.2 wt.% silicon.

The probability for LBE to penetrate and to get in contact with the grains in the IOZ increases with strain. The number and depth

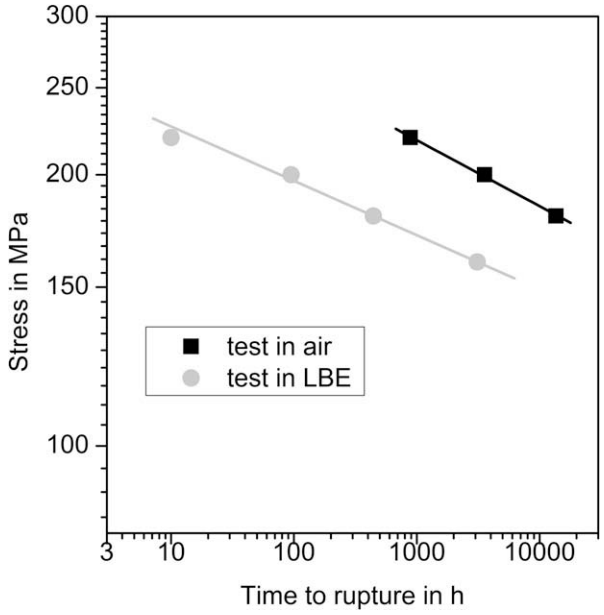

Fig. 11. Time to rupture of the samples tested in air and LBE at 160, 180, 200 and 220 MPa.

of microcracks increase and the degree of their healing decreases with increasing the applied stress (equivalent to high strain), with the result of a higher area of unprotected steel surface in direct contact with LBE. The steel surface area exposed to LBE increases furthermore, when LBE starts to disperse along the network of the pores located at the scale-steel interface. In this region the oxygen feed to LBE is hindered and it becomes impossible to form a new protective oxide layer. The attack, which occurs through a wetting-and-dissolution process of the Cr-depleted IOZ grains, initiates defects similar to short microcracks, ready to propagate into the bulk under applied stress [25]. Due to the reduction of the surface energy by Pb and Bi atom adsorption [16], the effective energy required for crack propagation will be reduced [15,17], enabling the microcracks to propagate at much higher speed [26].

At this point one can assume that, without scale cracking leading finally to the direct contact with LBE, the steel behavior during creep tests in LBE and in air might be almost the same. If the oxide scale would be much thinner, denser and more ductile, it could withstand higher strain (stress) levels, without cracking. Furthermore, if the composition of the steel would permit a rapid healing, then the influence of the LBE on the creep strength of the steel could be reduced. Some methods of surface engineering could offer valuable solutions to accomplish such goals. As shown in previous works, surface alloying with aluminum using, e.g. GESA pulsed large area electron beam, changes the oxidation behavior of T91 steel exposed to LBE, by forming thin and dense oxide scales [27].

5. Summary and conclusions

Uniaxial creep-to-rupture tests were performed on T91 steel in air and in flowing lead–bismuth eutectic melts (550 °C, 10^{-6} wt.% oxygen, flow rate of 0.5 m/s) at stress levels of 140, 160, 180, 200 and 220 MPa. Compared with specimens tested in air, the specimens tested in liquid–metal show: (i) an increase of the strain and the strain rate up to a factor of 53 (strain rate); (ii) a decrease of the time-to-rupture; (iii) a rapid transition into the third stage of creep at high stress (above 180 MPa). The analysis of the creep test results revealed several important surface phenomena, which lead to different behavior of the specimens tested in lead–bismuth eu-

tectic melts, compared with the specimens tested in air: (i) oxide scale breaking and crack propagation; (ii) liquid–metal–steel interaction at the crack tips; (iii) dissolution of steel components. The weight, with which these phenomena influence the specimen behavior during creep-to-rupture tests in lead–bismuth eutectic melts, depends on the value of the applied stress, which, in turn, determines the exposure times. At high stress, and therefore high strain, the crack propagation process is mostly controlled by the reduction of the surface energy due to Pb and Bi adsorption on the steel surface. At low stress (140 and 160 MPa) and low strain, this process is delayed due to the competing mechanism of healing the oxide scale cracks.

Normal operating conditions of nuclear systems components, cooled with LBE, do not foresee stress levels similar to those used here. However, the above discussed results can be taken into account for HLM nuclear systems under abnormal conditions, where high stress levels might be encountered. The role of LBE and of oxygen content under these conditions should be kept in mind.

The threshold stress, below which LBE has no influence on the creep properties, must be examined. Below this level, the data obtained during creep tests in air can be extrapolated to estimate the creep behavior of the specimens exposed to LBE.

Acknowledgements

The authors would like to thank the EC and the ISTC for funding the work presented in this paper under the 'EUROTRANS' Project, No: FI6 W-CT-2004-516520 and the ISTC project 2048, respectively.

References

[1] U. Knebel, H. Aït Abderrahim, L. Cinotti, F. Delage, C. Fazio, M. Giot, B. Giraud, E. Gonzalez, G. Granget, S. Monti, A.C. Mueller, European research programme for the transmutation of high level nuclear waste in an accelerator driven system, in: Proceedings of the FISA 2006, Luxembourg, 13–16 March, 2006.
[2] L. Cinotti, C. Fazio, J. Knebel, S. Monti, H. Ait Abderrahim, C. Smith, K. Suh, LFR "lead fast reactor", in: Proceedings of the FISA 2006, Luxembourg, 13–16 March, 2006.
[3] Handbook on Lead–Bismuth Eutectic Alloy and Lead Properties, Materials Compatibility, Thermal-Hydraulics and Technologies, ISBN: 978-92-64-99002-9, OECD 2007 <http://www.nea.fr/html/science/reports/2007/nea6195-handbook.html>.
[4] B.F. Gromov, Y.I. Orlov, P.N. Martynov, V.A. Gulevski, in: Proceedings of Heavy Liquid Metal Coolants in Nuclear Technology, HLMC'98, October 5–9, 1998, Obninsk, Russia, 1999, p. 87.
[5] G.S. Yachmenyov, A.Ye. Rusanov, B.F. Gromov, Yu.S. Belomytsev, N.S. Skortsov, A.P. Demishonkov, in: Proceedings of Heavy Liquid Metal Coolants in Nuclear Technology, HLMC'98, October 5–9, 1998, Obninsk, Russia, 1999, p. 133.
[6] G. Müller, G. Schumacher, F. Zimmermann, J. Nucl. Mater. 278 (1) (2000) 85.
[7] L. Soler, F.J. Martin, F. Hernandez, D. Gomez-Briceno, J. Nucl. Mater. 335 (2004) 174.
[8] G. Müller, A. Heinzel, J. Konys, G. Schumacher, A. Weisenburger, F. Zimmermann, V. Engelko, A. Rusanov, V. Markov, J. Nucl. Mater. 335 (2004) 163.
[9] C. Fazio, G. Benamti, C. Martini, G. Palombarini, J. Nucl. Mater. 296 (2001) 243.
[10] L. Martinelli, T. Dufrenov, K. Jaakou, A. Rosanov, F. Balbaud-Celerier, J. Nucl. Mater. 376 (2008) 282.
[11] A. Legris, G. Nicaise, J.-B. Vogt, J. Foct, J. Nucl. Mater. 301 (2002) 70.
[12] J.-B. Vogt, G. Nicaise, A. Legris, J. Foct, J. Phys. IV France 12 (2002) 8.
[13] W. Rostocker, J.M. McCaughey, H. Markus, in: Embrittlement by Liquid Metals, Reihold Publishing Corporation, New York, 1960. Chapman and Hall, Ltd., London.
[14] B. Joseph, M. Picat, F. Barbier, Eur. Phys. J. AP5 (1999) 19.
[15] E.E. Glickman, Multiscale Phenomena in Plasticity, NATO ASI Series E 367 (2000) 383.
[16] P.A. Rebinder, in: Proceedings of the Sixth Conference of Russian Physicists, Compendium of Lectures, Gosizdat, Moscow, 1928, p. 29 [in Russian].
[17] S. Guerin, J.-L. Pastol, C. Leroux, D. Gorse, J. Nucl. Mater. 318 (2003) 339.
[18] A.A. Griffith, Philos. Trans. R. Soc. A 221 (1921) 163.
[19] R.R. Hough, R. Rolls, J. Mater. Sci. 6 (1971) 1493.
[20] N.S. Stoloff, T.L. Johnston, Acta Metall. 11 (1963) 251.
[21] D. Gorse et al., Effect of LBE and lead on mechanical properties of structural materials, in: Lead–Bismuth Eutectic Alloy and Lead Properties, Materials Compatibility, Thermal-Hydraulics and Technologies, OECD/NEA, 2007, pp. 275–359, ISBN: 978-92-64-9902-9 (Chapter 7).
[22] J. Van den Bosch et al., EC FP6 EUROTRANS Project FI6W-CT-2004-516520, Deliverable 4.2, SCK-CEN, 2005.
[23] G. Diego et al., EC FP5 SPIRE Project FIS5-1999-00223, Deliverable 4, CIEMAT, 2001.
[24] A.D. Kashtanov, V.S. Lavrukhin, V.G. Markov, V.A. Yakovlev, S.N. Bozin, V.N. Leonov, B.S. Rodchenkov, A.I. Filin, Atom. Energy 97 (2004) 538.
[25] J.-B. Vogt, A. Verleene, I. Serre, F. Balbaud-Celerier, L. Martinelli, A. Terlain, J. Nucl. Mater. 14 (2007) 1185.
[26] Y. Day, B. Long, F. Groeschel, J. Nucl. Mater. 356 (2006) 222.
[27] A. Weisenburger, A. Heinzel, G. Mueller, H. Muscher, A. Rousanov, J. Nucl. Mater. 376 (2008) 274.